

# Probabilistic seismic hazard assessment for Taiwan: TEM PSHA2020

Earthquake Spectra

2020, Vol. 36(S1) 137–159

© The Author(s) 2020

Article reuse guidelines:

[sagepub.com/journals-permissions](https://sagepub.com/journals-permissions)

DOI: 10.1177/8755293020951587

[journals.sagepub.com/home/eqs](https://journals.sagepub.com/home/eqs)

Chung-Han Chan<sup>1,2</sup>, Kuo-Fong Ma<sup>1,2,3</sup>, J Bruce H Shyu<sup>4</sup>,  
Ya-Ting Lee<sup>1,2</sup>, Yu-Ju Wang<sup>5</sup>, Jia-Cian Gao<sup>6</sup>,  
Yin-Tung Yen<sup>7</sup> , and Ruey-Juin Rau<sup>8</sup>

## Abstract

The Taiwan Earthquake Model (TEM) published the first version of the Taiwan probabilistic seismic hazard assessment (named TEM PSHA2015) 5 years ago. For updating to the TEM PSHA2020, we considered an updated seismogenic structure database, including the structures newly identified with 3D geometry, an earthquake catalog made current to 2016, state-of-the-art seismic models, a new set of ground motion prediction equations, and site amplification factors. In addition to earthquakes taking place on each individual seismogenic structure, the updated seismic model included the possibility of an earthquake occurring on multiple structures. To include fault memory for illustrating activity on seismogenic structure sources, we incorporated the Brownian passage time model. For the crustal seismicity that cannot be attributed to any specific structure, we implemented both area source and smoothing kernel models. A new set of ground motion prediction equations is incorporated. In addition to the calculation of hazard at engineering bedrock, our assessment included site amplification factors that competent authorities of governments and private companies could use to implement hazard prevention and reduction strategies.

## Keywords

Probabilistic seismic hazard assessment, Taiwan, the Taiwan Earthquake Model, multiple-structure rupture, Brownian passage time model

Date received: 20 July 2020; accepted: 22 July 2020

<sup>1</sup>Earthquake-Disaster & Risk Evaluation and Management (E-DREaM) Center, National Central University, Taoyuan City

<sup>2</sup>Department of Earth Sciences, National Central University, Taoyuan City

<sup>3</sup>Institute of Earth Sciences, Academia Sinica, Taipei City

<sup>4</sup>Department of Geosciences, National Taiwan University, Taipei City

<sup>5</sup>Department of Nuclear Backend Management, Taiwan Power Company, Taipei City

<sup>6</sup>Institute of Applied Geology, National Central University, Taoyuan City

<sup>7</sup>Sinotech Engineering Consultants, Inc., Taipei City

<sup>8</sup>Department of Earth Sciences, National Cheng Kung University, Tainan City

## Corresponding author:

Chung-Han Chan, Earthquake-Disaster & Risk Evaluation and Management (E-DREaM) Center, National Central University, No. 300, Zhongda Rd., Zhongli Dist., Taoyuan City 32001.

Email: [hantijun@googlemail.com](mailto:hantijun@googlemail.com)

## Introduction

In 2015, the Taiwan Earthquake Model (TEM) proposed its first version of the probabilistic seismic hazard analysis (PSHA) for Taiwan, named TEM PSHA2015 (Wang et al., 2016a). This model adopted 38 seismogenic structures identified by Shyu et al. (2016), 28 shallow-area sources, 4 subduction-interplate sources, and 12 subduction-intraplate sources (Figure 3 of Wang et al., 2016a) to illustrate seismic activities in Taiwan and its vicinity. This assessment considered seismic hazard only for engineering bedrock, that is,  $V_s^{30}$  (i.e. averaged shear-wave velocity in the top 30 m) of 760 m/s, and therefore site amplification was neglected. Although such an assumption is straightforward for engineering applications, its application requires incorporating site amplification that could be overlooked by non-experts. The TEM PSHA2015 provided the first published national seismic hazard map of Taiwan, and it provided the ground basis for understanding the national seismic hazard potential. Several years after publishing this map, it was necessary to conduct advanced work that incorporated recent developments in PSHA practice and up-to-date data sets into a new PSHA model. Thus, this article details the official version of this model by the TEM team, named TEM PSHA2020.

To upgrade seismic hazard assessment properly, an evaluation of the TEM PSHA2015 seismic model was required. Chan et al. (2019) examined the performance of the TEM PSHA2015 through retrospectively forecasting the seismic behaviors of the 2018 Hualien, Taiwan, sequence and seismicity during 2012 and 2016. For seismogenic structure sources, the TEM PSHA2015 model forecasted a high earthquake probability of 53% in the coming 50 years on the Milun fault, which ruptured during this sequence. Its probability could be even higher by implementing a time-dependent Brownian passage time (BPT) model (probability of 80% in the coming 50 years), raising the importance of the BPT model for PSHA. Chan et al. (2019) also tested the shallow-background area sources of the TEM PSHA2015 model. Their study compared the shallow-background area sources with the Hualien sequence as well as the seismicity from 2012 to 2016 and confirmed their positive correlation through a Molchan diagram (Molchan, 1990). This test implies the shallow-background area model could forecast long-term seismic activity, applicable for subsequent PSHA models. Note that Chan et al. concluded similar forecasting reliability between the area sources in the TEM PSHA2015 model and the smoothing model of Woo (1996) although the spatial patterns of these two models are significantly different. Also, after announcing the TEM PSHA2015, the TEM seismogenic structures database was updated, including adding six newly identified structure sources (ID 39-44 in Table 1, structure alignments shown in Figure 1a), and revising the geometries of some structures from fixed dip angles (planar geometries) to depth-dependent dip angles (three-dimensional geometries). In addition, based on the TEM historical earthquake database (<http://tec.earth.sinica.edu.tw/TEM/hisevent/hisdoc.php>) and seismogenic structure alignments, potential ruptures on multiple structures have been identified, and corresponding parameters have been summarized in Table 2.

The understanding gained from the tests and use of the updated database could improve the quality of PSHA for Taiwan. First, we implemented an updated seismogenic structure database, including the consideration of earthquakes from multiple-segment ruptures. Considering the memory time-elapse of last rupture, we evaluated the time-dependent rupture probability for seismogenic structures. For shallow-background sources, we revised parameters for the area sources based on the updated earthquake catalog. In addition to the area source model, the background seismicity rate is also represented in the form of a smoothing model. To better model ground-shaking behaviors, we

**Table 1.** The source parameters for the 44 seismogenic structures in the TEM database.

ID	Seismogenic structure name	Type	Length (km)	Depth 1 (km)	Dip 1 (°) between depth 0 and 1	Depth 2 (km)	Dip 2 (°) between depth 1-2	Depth 3 (km)	Dip 3 (°) between depth 2 and 3	Width Area (km <sup>2</sup> )	M <sub>w</sub>	Displacement (m)	Slip rate (mm/year)	Recurrence interval (year)
1	Shanchiao fault	N	53.10	7.0	60	10.0	45	14	30	19.84	1053.50	7.01	1.29	780
2	Shuanglienpo structure	R	11.00	3.0	45	5.0	15	-	-	11.97	131.67	6.24	0.72	5540
3	Yangmei structure	R	22.10	3.0	60	-	-	-	-	3.46	76.47	6.03	0.60	3330
4	Hukou fault	R	25.60	10.0	30	-	-	-	-	20.00	512.00	6.77	1.16	2520
5	Fengshan river strike-slip structure	SS	30.60	13.8	85	-	-	-	-	13.90	425.34	6.66	0.95	300
6	Hsinchu fault	R	14.50	10.0	45	-	-	-	-	14.14	205.03	6.41	0.83	1260 (2823)
7	Hsincheng fault	R	28.50	12.9	30	-	-	-	-	25.71	732.74	6.91	1.31	1170
8	Hsinchu frontal structure	R	12.10	10.0	30	-	-	-	-	20.00	242.00	6.48	0.90	620 (1351)
9	Touhuanping structure	SS	25.80	12.0	85	-	-	-	-	12.05	310.89	6.52	0.80	6150 (15,166)
10	Miaoli frontal structure	R	30.90	10.0	30	-	-	-	-	20.00	618.00	6.84	1.22	660 (1383)
11	Tunglo structure	R	15.70	3.5	30	-	-	-	-	7.00	109.90	6.17	0.68	1360
12	East Miaoli structure	R	14.40	4.0	30	-	-	-	-	8.00	115.20	6.19	0.69	820
13	Shihtan fault	R	30.70	10.8	75	-	-	-	-	11.18	343.23	6.61	0.99	720 (1590)
14	Sanyi fault	R	29.80	9.0	15	-	-	-	-	34.77	1036.15	7.04	1.45	1710
15	Tuntzuchiao fault	SS	27.00	14.8	85	-	-	-	-	14.85	400.95	6.64	0.94	1880 (4105)
16	Changhua fault	R	82.20	3.0	45	5.0	30	12	10	48.55	3990.81	7.57	2.35	1260
17	Chelungpu fault	R	91.90	12.0	15	-	-	-	-	46.36	4260.48	7.60	2.45	350
18	Tamaopu—Shuangtung fault	R	69.20	6.0	30	-	-	-	-	12.00	830.40	6.96	1.38	1300
19	Chiuchungkeng fault	R	33.60	12.0	30	-	-	-	-	24.00	806.40	6.95	1.37	290
20	Meishan fault	SS	25.20	14.7	85	-	-	-	-	14.75	371.70	6.60	0.89	350 (16,869)

(continued)

Table 1. Continued

ID	Seismogenic structure name	Type	Length (km)	Depth I (km)	Dip I (°) between depth 0 and I	Depth 2 (km)	Dip2 (°) between depth 1-2	Depth 3 (km)	Dip3 (°) between depth 2 and 3	Width (km)	Area (km <sup>2</sup> )	M <sub>w</sub>	Displacement (m)	Slip rate (mm/year)	Recurrence interval (year)
21	Chiayi frontal structure	R	34.10	12.0	15	-	-	-	-	46.36	1580.88	7.21	1.71	3.36	510 (3006)
22	Muchilliao—Liuchia fault	R	26.40	12.0	30	-	-	-	-	24.00	633.60	6.85	1.23	5.75	210
23	Chungchou structure	R	29.20	12.0	30	-	-	-	-	24.00	700.80	6.89	1.28	12.20	100
24	Hsinhua fault	SS	14.80	15.0	85	-	-	-	-	15.06	222.89	6.38	0.69	2.65	260
25	Houchiali fault	R	12.20	5.0	45	-	-	-	-	7.07	86.25	6.07	0.61	7.07	90 (99,655)
26	Chishan fault	SS/R	40.00	10.8	75	-	-	-	-	11.18	447.20	6.68	0.97	1.10	880
27	Hsiaokangshan fault	R	11.10	7.0	30	-	-	-	-	14.00	155.40	6.30	0.75	1.78	420
28	Kaoping River structure	SS/R	33.40	12.3	75	-	-	-	-	12.71	424.51	6.66	0.95	0.32	2970
29	Chaochou fault	SS/R	99.30	11.1	75	-	-	-	-	11.50	1141.95	7.10	1.62	0.98	1650 (3481)
30	Hengchun fault	SS/R	41.90	15.0	75	-	-	-	-	15.53	650.71	6.85	1.20	6.15	200 (466)
31	Hengchun offshore structure	R	19.70	4.0	30	-	-	-	-	8.00	157.60	6.31	0.77	3.22	240
32	Milun fault	SS/R	32.60	10.0	75	-	-	-	-	10.35	337.41	6.56	0.85	10.15	80
33	Longitudinal Valley fault	R/SS	147.50	5.0	75	15.0	60	20	45	23.79	3509.02	7.52	2.25	11.35	200 (468)
34	Central Range structure	R	86.20	20.0	45	-	-	-	-	28.28	2437.74	7.38	2.00	7.28	270
35	Luyeh fault	R	19.60	2.0	45	4.0	30	-	-	6.83	133.87	6.24	0.71	5.28	130 (10,869)
36	Taimali coastline structure	R/SS	43.00	10.6	75	-	-	-	-	10.93	469.99	6.73	1.10	7.32	150
37	Northern Ilan structure	N	74.90	9.4	60	-	-	-	-	10.87	814.16	6.90	1.14	3.29	350
38	Southern Ilan structure	N	21.90	11.3	60	-	-	-	-	12.99	284.48	6.43	0.64	5.48	120

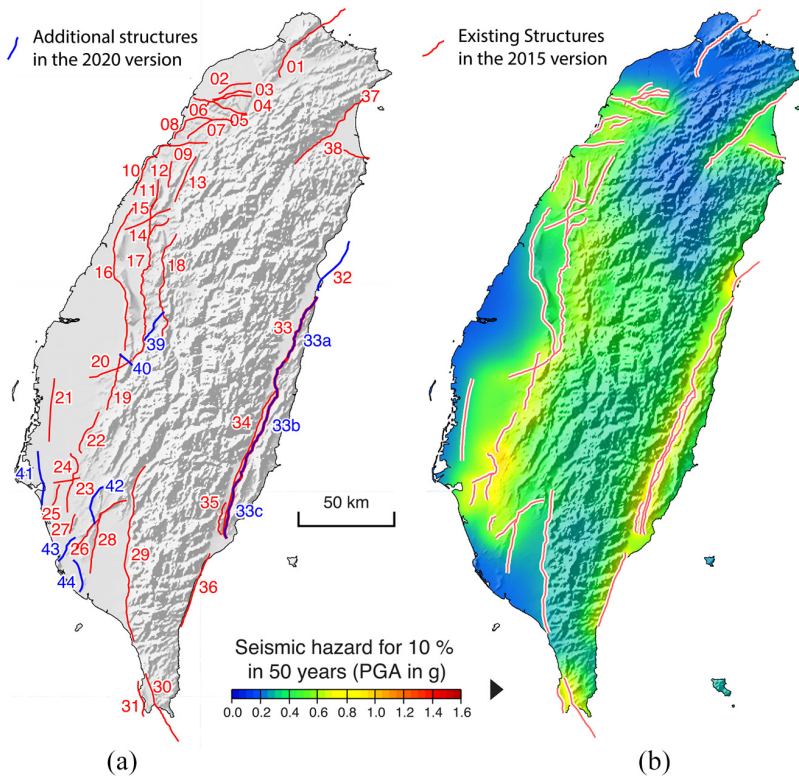
(continued)

Table 1. Continued

ID	Seismogenic structure name	Type	Length (km)	Depth 1 (km)	Dip 1 (°) between depth 0 and 1	Depth 2 (km)	Dip2 (°) between depth 1-2	Depth 3 (km)	Dip3 (°) between depth 2 and 3	Width (km)	Area (km <sup>2</sup> )	M <sub>w</sub>	Displacement (m)	Slip rate (mm/year)	Recurrence interval (year)
39	Chushiang structure	R/SS	19.80	3.0	55	-	-	-	-	3.66	72.47	6.00	0.57	5.01	110
40	Gukeng structure	SS	9.20	12.0	85	-	-	-	-	12.05	110.86	6.07	0.48	0.94	510
41	Tainan frontal structure	R	32.90	3.0	30	12.0	15	-	-	52.36	1722.64	7.24	1.74	0.92	1890 (9705)
42	Longchuan structure	R	23.10	12.0	60	-	-	-	-	13.86	320.17	6.58	0.96	1.73	550
43	Yuchang structure	R/SS	16.6	12.0	75	-	-	-	-	12.42	206.17	6.41	0.83	1.64	510
44	Fengshan hills frontal structure	R	19.1	15.0	30	-	-	-	-	30.00	573.00	6.81	1.19	0.92	1290

TEM: Taiwan Earthquake Model.

Based on this database, a seismogenic structure would fully rupture only during an earthquake with a characteristic magnitude shown in the table. That is, a partial rupture with a smaller magnitude is not considered from the seismogenic structure source. Note that some of the structures obtain depth-dependent dip angles. The recurrence intervals in parentheses were evaluated by considering slip partitioning for multiple-structure ruptures. The alignments of the seismogenic sources are presented in Figure 1a.



**Figure 1.** (a) Distribution of the 44 seismogenic structures in the TEM database and (b) TEM PSHA2015 map of PGA (in g) for 10% probability in 50 years. Note that TEM PSHA2015 implemented only 38 seismogenic structures (denoted as red alignments in (b)). Blue alignments represent newly identified structures incorporated in this study.

**Table 2.** Potential multiple-structure ruptures and structure segmentations with rupture type, corresponding rupture areas, magnitudes and recurrence intervals of potential earthquakes.

ID	Seismogenic structure name	Type	Area (km <sup>2</sup> )	$M_w$	Recurrence interval (year)
6, 8	Hsinchu fault, Hsinchu frontal structure	R, R	447.03	6.65	1483
9, 10	Touhuanping structure, Miaoli frontal structure	SS, R	928.89	6.92	1628
13, 15	Shihtan fault, Tuntzuchiaio fault	R, SS	744.18	6.83	1958
20, 21	Meishan fault, Chiayi frontal structure	SS, R	1952.58	7.24	1518
21, 41	Chiayi frontal structure, Tainan frontal structure	R, R	3303.52	7.43	1338
25, 41	Houchiali fault, Tainan frontal structure	R, R	1808.89	7.25	3279
29, 30	Chaochou fault, Hengchun fault	SS/R, SS/R	1792.66	7.20	904
35, 33c	Luyeh fault, Longitudinal Valley fault (south)	R, R/SS	940.35	6.97	897
33a	Longitudinal Valley fault (north)	R/SS	913.54	6.99	1792
33b	Longitudinal Valley fault (central)	R/SS	1789.01	7.26	904
33c	Longitudinal Valley fault (south)	R/SS	806.48	6.95	1983
33ab	Longitudinal Valley fault (north, central)	R/SS	2702.54	7.42	603
33bc	Longitudinal Valley fault (central, south)	R/SS	2595.49	7.40	634

The alignments of the seismogenic sources are presented in Figure 1a.

implemented a new set of ground motion prediction equations (GMPEs) for analysis. To incorporate site amplification, our assessment applied an  $V_s^{30}$  map and new GMPEs to describe site and path effects of strong ground motion attenuation. While we made the effort of the TEM PSHA2020 model for the practical application, the challenges and status of the TEM PSHA model for Taiwan continue required the long-term effort as addressed in Gerstenberger et al. (2020), which review the state of the art and future challenges of PSHA at regional and national scale.

## **Modification of seismogenic structure sources**

The TEM PSHA2015 (Wang et al., 2016a) concluded that the seismogenic structure sources are the main contributors to the seismic hazard (Figure 1b). In addition, Wang et al. (2016b) concluded that the parameter uncertainties of these seismogenic structure sources could result in significant deviations of evaluated hazard levels. Therefore, we applied a new model to illustrate their behaviors and minimize their uncertainties, which is detailed in the following sections.

### *Updated seismogenic structure database*

The TEM PSHA2015 implemented the seismogenic structure database summarized by Shyu et al. (2016), which incorporated 38 seismogenic structures with planar geometries and characteristic magnitudes, that is, a single magnitude and fixed recurrence interval for each structure. This database was updated (Shyu et al., 2020) to include six newly identified structure sources: the Chushiang, Gukeng, Tainan frontal, Longchuan, Youchang and Fengshan hills frontal structures (ID 39–44, respectively; corresponding fault alignment of each source is presented in Figure 1a). Also, based on additional evidence, such as seismic profiles, dip angles of some sources are suggested to be depth variable, with a gentler dipping at depth (Table 1). Surface traces of a few structures are also modified based on new data or field investigation results. For example, the Milun fault (ID 32) was extended northeastward, and with a longer length, its magnitude becomes larger (from M6.40 to M6.56). Note that a structure with a gentler dip angle within the seismogenic depth would have a larger magnitude and longer recurrence interval (a larger magnitude infers larger slip during an event, assuming a fixed slip rate).

Based on the new structure database, the new results of seismic hazards were evaluated (Figure 2a). Compared with the TEM PSHA2015 map (Figure 1b), the updated map shows significantly lower hazards along some faults that have longer return periods, such as the Shuanglienpo structure (ID 2), Yangmei structure (ID 3), Hukou fault (ID 4), Hsincheng fault (ID 6), Hsinchu frontal structure (ID 8), Miaoli frontal structure (ID 10), Tunglo structure (ID 11), Sanyi fault (ID 14), and Tuntzuchiao fault (ID 15). In contrast, this new assessment shows higher hazard levels in the vicinity of some newly identified structures (red alignments in Figure 2) that were not included in the TEM PSHA2015 model.

### *Multiple-structure rupture*

Although the TEM PSHA2015 assumed an earthquake takes place on only one individual seismogenic structure source, some historical earthquakes show that it is possible to have simultaneous ruptures on multiple seismogenic structures. Implementing the multiple-structure rupture factor could enable comprehension of some extreme cases in our hazard

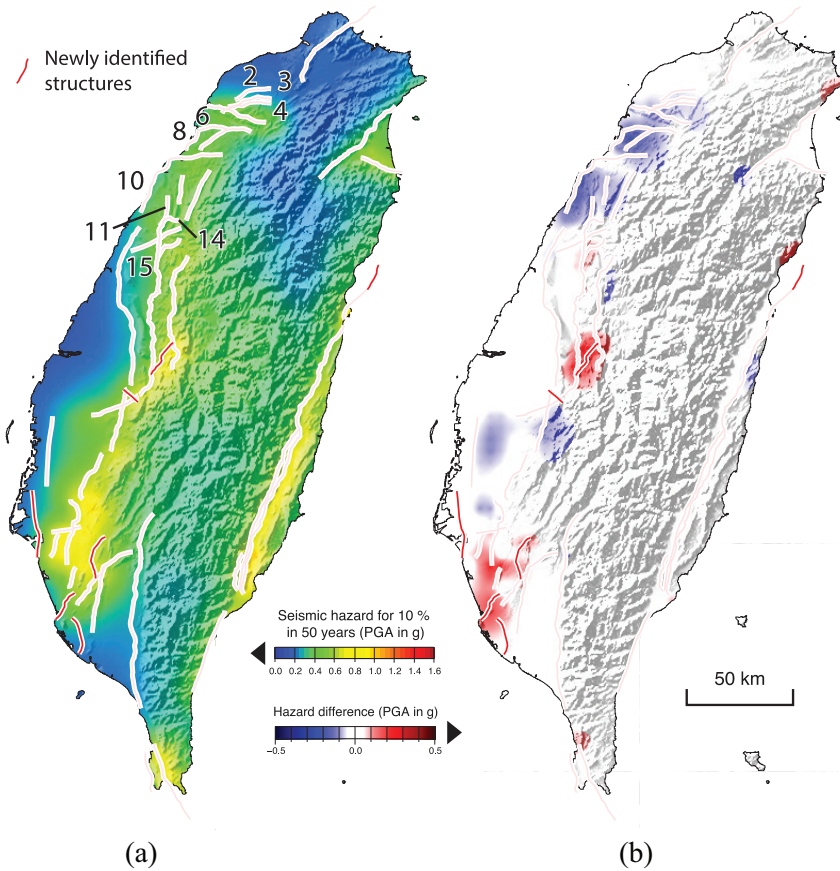


**Figure 2.** (a) The seismic hazard maps considering the new TEM seismogenic structure database, including six newly identified structure sources (denoted as dark red alignments) and 3D structure geometry and (b) the impact of this innovation. (b) The difference between Figures 2a and 1b. The unit of the PSHA is PGA (in g) for 10% probability in 50 years (i.e. recurrence interval of 475 years).

assessment. We considered several possible multiple-structure rupture cases (Table 2) for the hazard assessment based on historical records, for example, the Shihtan (ID 13) and Tuntzuchiao (ID 15) faults in the 1935  $M_w$  7.1 case, or geological relationships between neighboring structures, such as the Hsinchu fault (ID 6) and Hsinchu frontal structure (ID 8), and the Touhuanping (ID 9) and Miaoli frontal (ID 10) structures.

To incorporate this factor into seismic hazard assessment requires partitioning seismic moment rates into the cases of single- and multiple-structure ruptures. Here, we implemented the Gutenberg–Richter law (Gutenberg and Richter, 1944) to describe the relationship between earthquake magnitude  $M$  and frequency  $\dot{N}$  as follows:

$$\log(\dot{N}) = a - bM, \quad (1)$$

where the  $a$  and  $b$  values are constants that can be obtained through regression of earthquake activity. We followed the procedure of Wang et al. (2016a), who determined a  $b$  value for the Taiwan region through regression and obtained a  $b$  value of 1.10. Note that



the acquisition of the earthquake catalog, data processing and analysis of the Gutenberg–Richter law will be detailed later in the text.

Thus, the partitioned slip rates of the first and second structures (denoted as  $\dot{D}'_{L1}$  and  $\dot{D}'_{L2}$ , respectively) can be represented as

$$\dot{D}'_{L1} = \frac{\dot{D}_{L1}}{\left(\frac{A_{L1+L2}}{A_{L1}} \times C_1 + 1\right)} \quad (2)$$

and

$$\dot{D}'_{L2} = \frac{\dot{D}_{L2}}{\left(\frac{A_{L1+L2}}{A_{L2}} \times C_2 + 1\right)}, \quad (3)$$

respectively, where  $\dot{D}_{L1}$  and  $\dot{D}_{L2}$  represent the original slip rates of the first and second structures, respectively, available from Table 1;  $A_{L1}$  and  $A_{L2}$  represent the areas of the first and second structures, respectively, available from Table 1; and  $A_{L1+L2}$  represents the area of the multiple-structure rupture. In addition,  $C_1$  represents the partitioned rate between multiple- ( $\dot{D}_{L1+L2}^{L1}$ ) and single-structure ( $\dot{D}_{L1}$ ) ruptures from the first structure, represented as

$$C_1 = \frac{10^{b \times (M_{L1} - M_{L1+L2})} \times D_{L1+L2}}{D_{L1}} \quad (4)$$

and

$$\dot{D}_{L1+L2}^{L1} = C_1 \times \dot{D}'_{L1}, \quad (5)$$

where  $M_{L1}$  and  $M_{L1+L2}$  represent the magnitudes of the first structure and multiple-structure ruptures, respectively (available from Tables 1 and 2, respectively);  $D_{L1+L2}$  represents the slip of the multiple-structure rupture, available from Table 2; and  $D_{L1}$  represents the slip of the first structure, available from Table 1.  $C_2$  represents the partitioned rate between multiple- ( $\dot{D}_{L1+L2}^{L2}$ ) and single-structure ( $\dot{D}'_{L2}$ ) ruptures from the second structure, represented as

$$C_2 = \frac{10^{b \times (M_{L2} - M_{L1+L2})} \times D_{L1+L2}}{D_{L2}} \quad (6)$$

and

$$\dot{D}_{L1+L2}^{L2} = C_2 \times \dot{D}'_{L2}, \quad (7)$$

where  $M_{L2}$  represents the magnitude of the second structure, and  $D_{L2}$  represents the slip of the second structure (both available from Table 1).

Thus, the slip rate for the multiple-structure rupture,  $\dot{D}_{L1+L2}$ , can be represented as

$$\dot{D}_{L1+L2} = \dot{D}_{L1+L2}^{L1} + \dot{D}_{L1+L2}^{L2} \quad (8)$$

and its recurrence interval,  $R_{L1+L2}$ , can be represented as follows:

$$R_{L1+L2} = \frac{D_{L1+L2}}{\dot{D}_{L1+L2}}. \quad (9)$$

Through this approach, the recurrence intervals of the first and second structures ( $R_{L1}$  and  $R_{L2}$ , respectively) are estimated based on the partitioned slip rates, represented as

$$R_{L1} = \frac{D_{L1}}{\dot{D}'_{L1}} \quad (10)$$

and

$$R_{L2} = \frac{D_{L2}}{\dot{D}'_{L2}}, \text{ respectively.} \quad (11)$$

For the case of the Hsinchu fault (ID 6) and Hsinchu frontal structure (ID 8) as an example,

$$\begin{aligned} C_1 &= 10^{1.1 \times (6.41 - 6.65)} \times 0.87 / 0.83 = 0.57 \text{ (for the Hsinchu fault);} \\ \dot{D}'_{L1} &= 0.66 / ((447.03 / 205.03) \times 0.57 + 1) = 0.294 \text{ m;} \\ \dot{D}'_{L1+L2} &= 0.57 \times 0.294 = 0.168 \text{ mm/year;} \\ C_2 &= 10^{1.1 \times (6.48 - 6.65)} \times 0.87 / 0.90 = 0.628 \text{ (for the Hsinchu frontal structure);} \\ \dot{D}'_{L2} &= 1.44 / ((447.03 / 242.00) \times 0.628 + 1) = 0.666 \text{ m;} \\ \dot{D}'_{L1+L2} &= 0.628 \times 0.666 = 0.419 \text{ mm/year;} \\ \dot{D}_{L1+L2} &= 0.168 + 0.419 = 0.587 \text{ mm/year;} \\ R_{L1+L2} &= 0.87 / 0.587 = 1483 \text{ years (recurrence interval of the multiple-structure rupture);} \\ R_{L1} &= 0.83 / 0.29 \times 1000 = 2823 \text{ years (new recurrence interval of the Hsinchu fault);} \\ R_{L2} &= 0.90 / 0.67 \times 1000 = 1351 \text{ years (new recurrence interval of the Hsinchu frontal} \\ &\text{structure).} \end{aligned}$$

Considering multiple-structure rupture cases did not result in a significant difference in the hazard level for a short return period (i.e. 475 years, corresponding to a 10% probability in 50 years), since the return periods for the multiple-structure ruptures are usually long. However, this factor becomes crucial when a PSHA return period is assumed to be longer (i.e. the case of 2475 years as shown in Figure 3). For example, hazard levels become higher in the vicinity of the Chaochou fault (ID 29) and Tainan frontal structure (ID 41).

### *Time-dependent rupture possibility model*

For the rupture probability of the seismogenic structure sources, the TEM PSHA2015 model followed a Poisson distribution, assuming faults do not remember time-elapses of previous ruptures. Such an assumption, however, has been questioned in some PSHA studies (e.g. Chan et al., 2017).

To evaluate time-dependent rupture possibilities for the seismogenic structure sources, we adopted the BPT model (Ellsworth et al., 1999), which included occurrence time of last rupture. This model has been applied to other seismic hazard assessments, for example, the

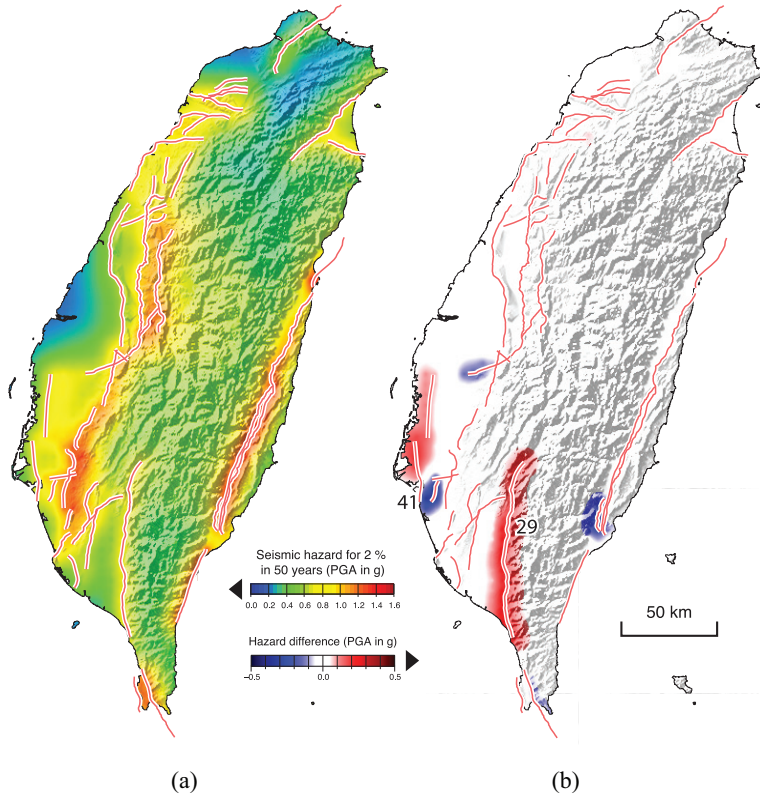


**Figure 3.** (a) The seismic hazard maps considering the possibility of an earthquake on multiple seismogenic structures and (b) the impact of this innovation. (b) The difference between Figures 3a and 2a. The unit of the PSHA is PGA (in g) for 2% probability in 50 years (i.e. recurrence interval of 2475 years). The locations of the Chaochou fault (ID 29) and Tainan frontal structure (ID 41) are denoted.

National Seismic Hazard Maps for Japan (Fujiwara, 2014). The density function ( $DF$ ) of the BPT model can be expressed as follows:

$$DF = \left( \frac{\mu}{\pi\alpha^2 t^3} \right)^{1/2} \exp\left( -\frac{(t - \mu)^2}{2\alpha^2 \mu t} \right), \quad (12)$$

where  $\mu$  represents the mean recurrence interval,  $t$  represents the time elapsed since the last rupture of the event, and  $\alpha$  represents the aperiodicity, usually between 0.3 and 0.7. Chan et al. (2017) applied this model to the seismogenic structures in Taiwan and tested the deviations of rupture probability and seismic hazard contributed by  $\alpha$  using its two end members. Their results show that the rupture probability differences for most cases are less than 20% (Table 6 of Chan et al., 2017) and less than 2% of the entire study area with a hazard level difference of more than 0.1 g (Figure 3 of Chan et al., 2017). This test suggested an insignificant variance in hazard levels within a reasonable  $\alpha$ . Thus, we assumed a median value of 0.5 in our study.

**Table 3.** Rupture probabilities and relative rate differences determined by different models at the time snapshots of 2018 based on corresponding recurrence intervals and time elapsed since the last event.

Fault name	ID	Recurrence interval (years)	Time-independent rate (%)	Time elapsed	Time-dependent rate (%)	Rate change (%)
Shihtan fault	13	516	97.9	82	0.2	-97.2
Tuntzuchiao fault	15	880	96.4	82	0.0	-100.0
Changhua fault	16	303	95.6	169	20.3	37.8
Chelungpu fault	17	371	12.6	18	0.0	-99.9
Meishan fault	20	347	91.8	111	7.2	-47.8
Muchiliao—Liuchia fault	22	212	89.7	155	34.4	78.9
Hsinhua fault	24	245	87.5	71	10.2	-47.2
Milun fault	32	189	23.2	66/0	80.8/38.0	507.6/-35.9
Longitudinal Valley fault	33	189	23.2	66	19.2	-13.9

BPT: Brownian passage time.

The time-dependent and time-independent rates are estimated according to the BPT and Poisson models, respectively. The alignments of the seismogenic sources are presented in Figure 1a.

To utilize the previous rupture events on specific seismogenic structure sources, we accessed the TEM historical earthquake database (<http://tec.earth.sinica.edu.tw/TEM/hisevent/hisdoc.php>) for the time and the corresponding sources of past earthquakes (Table 3). We started with 2018 and calculated rupture probability for the next 50 years. The BPT model suggests higher rupture probabilities for the seismogenic structures that have longer time elapsed with shorter recurrence intervals, such as the Changhua (ID 16), Muchiliao-Liuchia (ID 22), and Milun (ID 32) faults. In contrast, earthquake probabilities for the structures that have ruptured recently become lower, such as the Shihtan (ID 13) and Tuntzuchiao (ID 15) faults that ruptured in 1935, and the Chelungpu fault (ID 17), which ruptured in 1999.

With the time elapsed since the last rupture and the averaged recurrence intervals for the source, the BPT distribution provides rupture probabilities, and the seismic hazard can be assessed accordingly (Figure 4). This model suggests a higher hazard near the seismogenic structures that have longer time elapsed with shorter recurrence intervals, such as the Muchiliao-Liuchia (ID 22) and Milun (ID 32) faults. The earthquake probabilities for the structures that have ruptured recently, however, become lower, such as the Shihtan (ID 13), Tuntzuchiao (ID 15), and Chelungpu (ID 17) faults, resulting in a lower hazard level in central Taiwan (Figure 4).

## Modification of shallow-background sources

Besides seismogenic structures, another category of seismic sources in the crust is the shallow-background source. This category covers earthquakes that do not take place in seismogenic structures. The TEM PSHA2015 model proposed area sources to present the seismicity in Taiwan and its vicinity (Figure 5). Based on this model, the seismicity rate inside each zone is spatial homogeneous and is obtained by regression of the seismicity in 1973–2011 by the Gutenberg-Richter law (Gutenberg and Richter, 1944, Equation 1 of this study). In our current study, we renew the area source model with an updated catalog and also propose a smoothing model, described in the following.

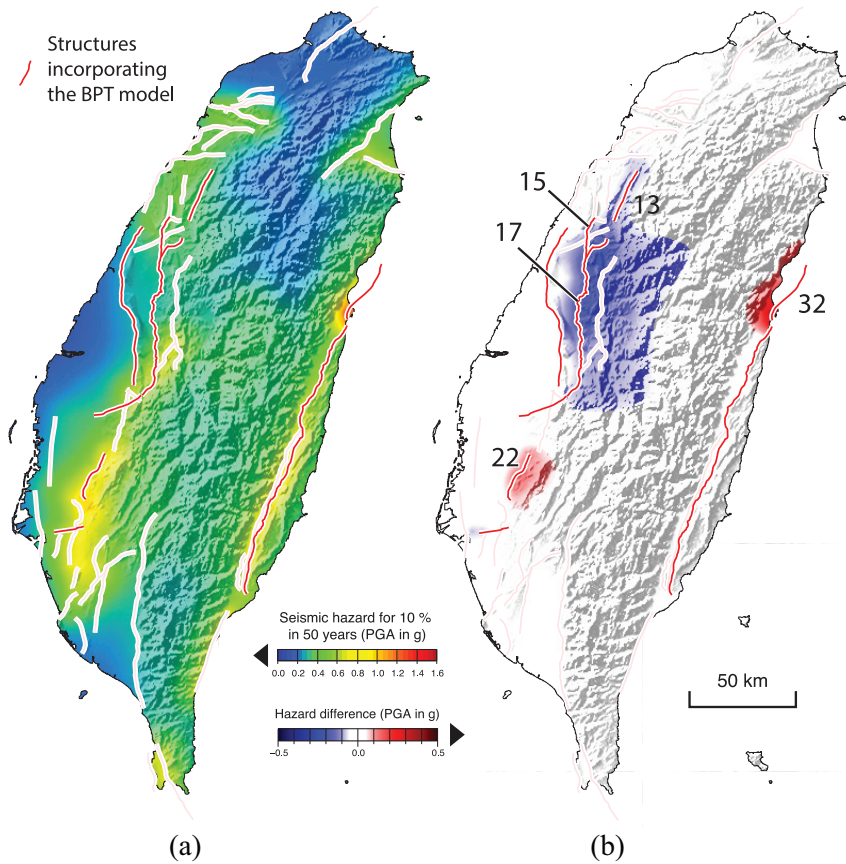


**Figure 4.** (a) The seismic hazard maps considering the BPT model and (b) the impact of this innovation. (b) The difference between Figures 4a and 3a. The unit of the PSHA is PGA (in g) for 10% probability in 50 years (i.e. recurrence interval of 475 years). The structures incorporating the BPT model are denoted as dark red alignments. The location of the Chelungpu (ID 17), Muchiliao-Liuchia (ID 22), and Milun (ID 32) faults is denoted.

### Implementing the updated earthquake catalog

To precisely illustrate the shallow-background source, it is crucial to implement reliable earthquake parameters (i.e. hypocenter, magnitude) from a high-quality earthquake catalog. We acquired the database by Wu et al. (2008), which relocates the parameters based on the records of the Central Weather Bureau Seismic Network (CWBSN). To conduct a reliable regression, only the complete part of the catalog was implemented. Thus, we followed the suggestion of Chen et al. (2013), using the earthquakes with  $M \geq 4.0$  from 1973 to 1993 and  $M \geq 3.0$  from 1993 to 2016, based on the update of the Wu et al. database, for subsequent analyses. Since our shallow-background source model represents only seismicity activity in the shallow crust, we excluded the earthquakes with hypocentral depth larger than 30 km, which are attributed to subduction intraplate sources (Wang et al., 2016a). To keep the model following the Poissonian distribution (earthquakes are independent of each other), we removed foreshocks and aftershocks from the catalog based on the declustering approach proposed by Gardner and Knopoff (1974). Note that

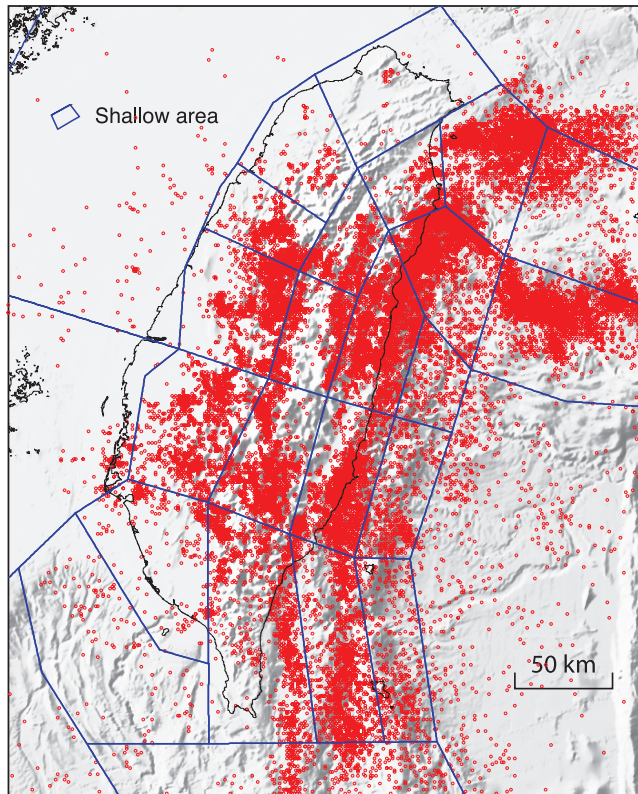


**Figure 5.** Distribution of the 28 area sources and seismicity implemented in this study. The earthquakes' parameters were obtained from the CWBSN catalog. We considered only the earthquakes with  $M \geq 4.0$  from 1973 to 1993 and  $M \geq 3.0$  from 1993 to 2016. Foreshocks and aftershocks in the catalog were removed based on the declustering approach proposed by Gardner and Knopoff (1974).

our study did not consider epistemic uncertainty resulting from various declustering approaches. The analyzed earthquake catalog is shown in Figure 5 and was implemented for constructing shallow-background source models, including area source and smoothing models.

### *Area source model*

Presenting an area source model requires the definition of the geometry for each area source. We followed the definition of the TEM PSHA2015, which defines 28 area sources in Taiwan and its neighboring region (blue polygons in Figure 5). We described the seismicity for each area source based on the Gutenberg-Richter law (Gutenberg and Richter, 1944) by regression of the catalog. Following the procedure of the TEM PSHA2015 (Wang et al., 2016a), we first obtained a unified  $b$  value of 1.10 for the Taiwan region. Then we determined the  $a$  value for each area (Table 4). By implementing the  $a$  and  $b$  values of each area, seismicity density can be estimated and plotted, shown in Figure 6a. Based on this area source model combined with the models illustrating other seismogenic sources, the seismic hazard for Taiwan can be assessed (Figure 6c). It shows a low hazard level in the region with small  $a$  values and corresponding seismicity densities (such as S04).

**Table 4.**  $a$  and  $b$  values, size (in km), and earthquake density for  $M \geq 4.0$  for 28 area sources.

Area	$a$ value	$b$ value	Size (km)	Density ( $M \geq 4$ per km <sup>2</sup> )
S01	4.090	1.100	37,289	1.31E-05
S02	4.480	1.100	16,356	7.35E-05
S03	4.010	1.100	14,025	2.90E-05
S04	3.450	1.100	4277	2.62E-05
S05A	3.960	1.100	2656	1.37E-04
S05B	4.750	1.100	1917	1.17E-03
S06	5.470	1.100	3402	3.45E-03
S07	5.260	1.100	3817	1.90E-03
S08A	4.710	1.100	4316	4.73E-04
S08B	4.050	1.100	6991	6.39E-05
S09	4.940	1.100	1589	2.18E-03
S10	5.230	1.100	1879	3.60E-03
S11	5.120	1.100	2892	1.81E-03
S12	5.230	1.100	5969	1.13E-03
S13	4.950	1.100	8706	4.07E-04
S14A	4.830	1.100	1616	1.66E-03
S14B	5.420	1.100	3207	3.26E-03
S14 C	5.240	1.100	4626	1.49E-03
S15	5.730	1.100	2819	7.58E-03
S16	5.940	1.100	5178	6.69E-03
S17A	5.630	1.100	2740	6.19E-03
S17B	4.720	1.100	1407	1.48E-03
S18A	5.420	1.100	2806	3.73E-03
S18B	4.890	1.100	2205	1.40E-03
S19A	5.500	1.100	3551	3.54E-03
S19B	4.880	1.100	2786	1.08E-03
S20	4.910	1.100	14,624	2.21E-04
S21	5.380	1.100	28,197	3.39E-04

The  $a$  and  $b$  values were obtained using regression of earthquake parameters as recorded by the CWBSN from 1973 to 2016. The geometries of the area sources are presented in Figure 5.

### Smoothing model

Besides the area source model mentioned above, we implemented another seismogenic model for the background seismicity based on the smoothing approach proposed by Woo (1996). Unlike an area source model, it does not require a subjective definition of area source geometry, which might result in epistemic uncertainty (Chan et al., 2019). This approach summarizes seismic activity in an earthquake catalog based on the smoothing kernel, which can be represented as a function of the magnitude  $M$  and the distance between the site of interest and the epicenter of the  $i$ th earthquake, shown as follows:

$$K(M, x - x_i) = \frac{PL - 1}{\pi H^2(M)} \left( 1 + \left( \frac{x - x_i}{H(M)} \right)^2 \right)^{-PL}, \quad (13)$$

where  $PL$  denotes the power law index. The bandwidth function  $H(M)$  is defined as the mean distance between each event with magnitude  $M$  and its nearest neighbor, represented as follows:

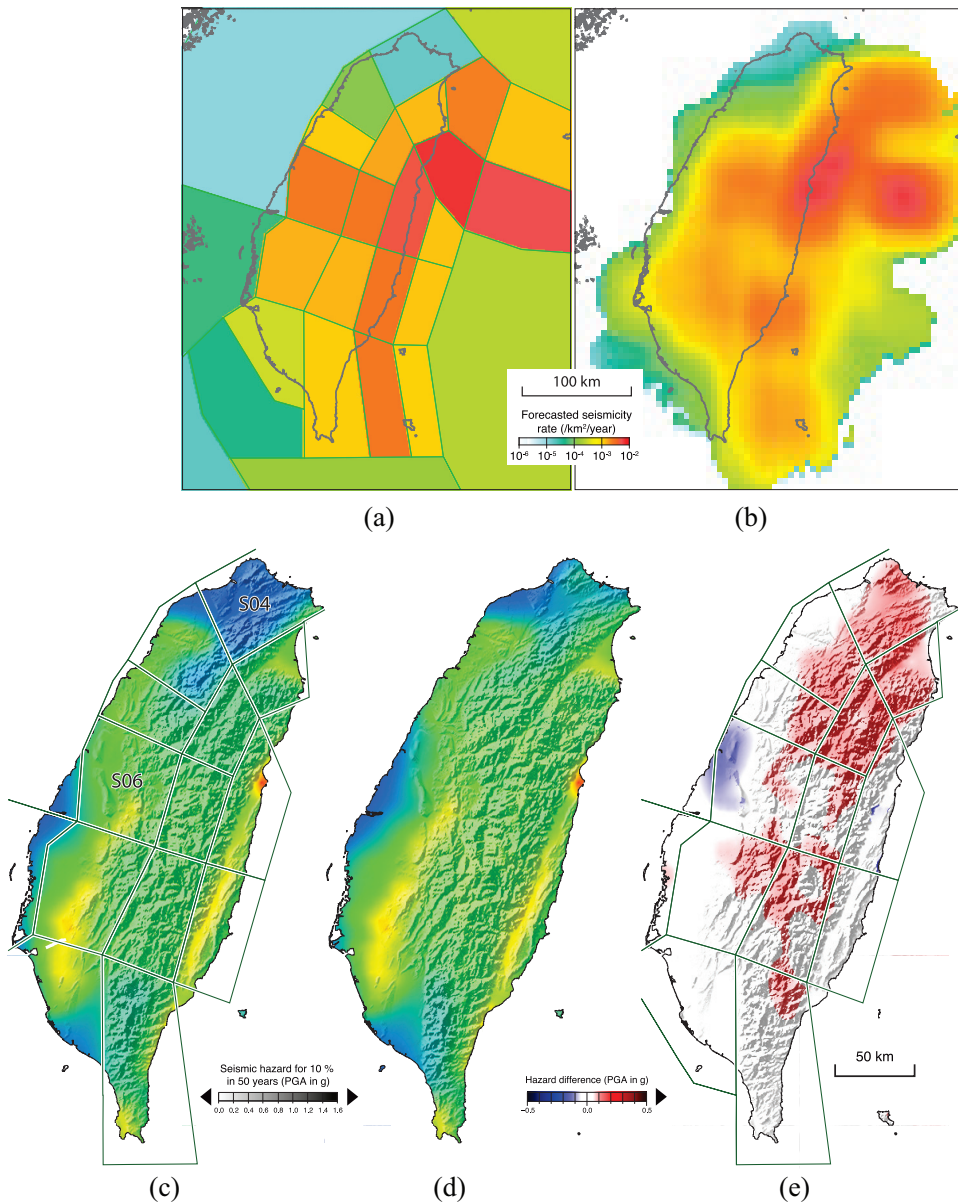


**Figure 6.** Distribution of seismicity density evaluated by (a) the area source model and (b) the smoothing approach of Woo (1996), and the seismic hazard maps considering (c) the area source and (d) the smoothing model, respectively, for shallow-background seismicity. (e) The difference between (c) and (d). The unit of the PSHA is PGA (in g) for 10% probability in 50 years (recurrence interval of 475 years). The locations of S04 and S06 are denoted.

$$H(M) = c \cdot e^{d \cdot M}, \quad (14)$$

where  $c$  and  $d$  are constants that can be obtained by regression. Through analyzing the catalog mentioned in the previous section, we determined that the  $c$  and  $d$  values of the



bandwidth function are 0.0146 and 1.1893, respectively. Thus, a seismic density model can be proposed accordingly (Figure 6b), and the seismicity hazard can be subsequently assessed (Figure 6d). Compared to the area source model (Figure 6c), implementing the smoothing model obtained a higher hazard level in central-northern Taiwan and a lower hazard at the western edge of S06 (Figure 6e). Such discrepancies could be attributed to the spatial heterogeneity of the seismicity (Figure 5), which can be presented by a smoothing model but would be averaged based on the area source model. Since Chan et al. (2019) concluded similar levels of earthquake forecasting ability between the area source and smoothing models, the TEM PSHA2020 model considered both models and assumed equal weightings (50% for each) in the logic tree for the assessment.

## Site effect

The TEM PSHA2015 did not include site effect, that is, its outcomes represented hazard levels for engineering bedrock. Thus, application of the TEM PSHA2015 hazard map required accessing site amplification for the sites of interest. Such a requirement could confuse non-experts who do not have either an engineering or scientific background. For easier application for end users, our assessment included built-in site amplification that requires an  $V_s^{30}$  map. We obtained the  $V_s^{30}$  at the 816 sites of the Taiwan Strong Motion Instrumentation Program (TSMIP) stations from the Engineering Geological Database for TSMIP (<http://egdt.ncree.org.tw/>) (solid circles with colors denoting  $V_s^{30}$ ). In this database, the  $V_s^{30}$  at most sites are obtained from measurements (Kuo et al., 2012), whereas some are acquired by estimation. Detailed parameters for each site can be accessed through [http://egdt.ncree.org.tw/DataList\\_eng.htm](http://egdt.ncree.org.tw/DataList_eng.htm). After interpolation based on these data, we obtained an  $V_s^{30}$  map with a resolution of 500 by 500 m<sup>2</sup> (Figure 7c). This map shows low  $V_s^{30}$  at some plains and basins, for example, Taipei Basin, Ilan Plain, and Chianan Plain. Based on the implemented GMPEs by Lin (2009), the low  $V_s^{30}$  results in significant site amplification and elevated seismic hazard (Figure 7d).

## GMPE

For a seismic hazard assessment, illustrating ground-shaking behaviors requires GMPEs representing the ground-shaking level as a function of magnitude, distance, and other factors. In the TEM PSHA2015, the implemented GMPEs for the crustal events are those by Lin (2009) that were obtained based on the observations of the Taiwan events. This GMPE set, however, has been criticized for overestimation in the near-field cases (Reevaluation of Probabilistic Seismic Hazard of Nuclear Facilities in Taiwan Using SSHAC Level 3 Methodology, <http://sshac.ncree.org.tw>). Our current study implemented the GMPEs proposed by Lin et al. (2011) instead, which are also obtained based on Taiwan observations, but have corrected near-field bias. We are aware that after the framework of TEM PSHA2020 was determined, some references were published describing new sets of GMPEs based on the observations of the crustal events and earthquakes in Taiwan (e.g. Chao et al., 2020; Phung et al., 2020). These new GMPEs will be incorporated in the next generation of the TEM PSHA.

By incorporating the GMPEs of Lin et al. (2011), the seismic hazard (Figure 8) shows lower levels in the region close to some of the seismogenic structures in the plain regions with low  $V_s^{30}$  (Figure 7c).

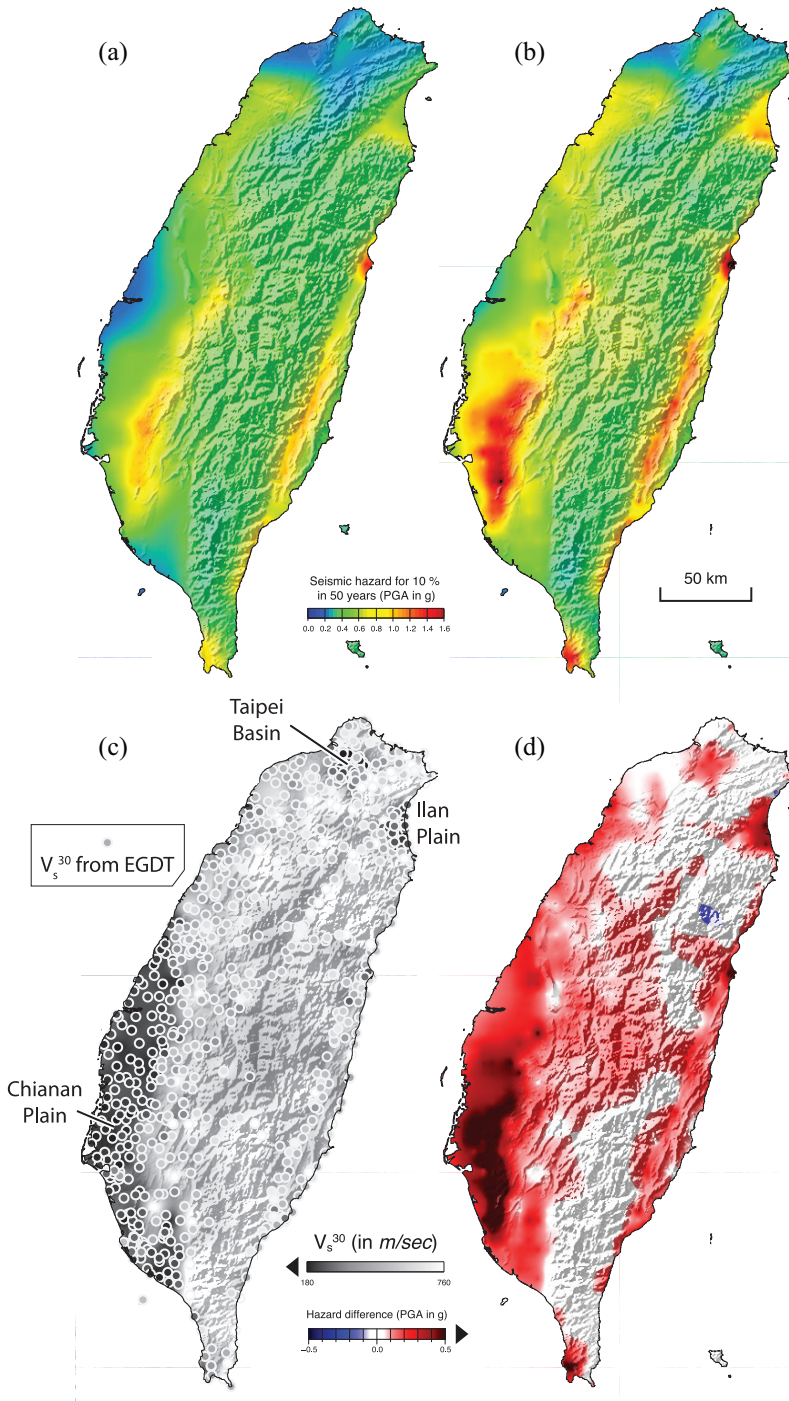


**Figure 7.** The seismic hazard maps considering (a) engineering bedrock and (b) site amplification using the factor of  $V_s^{30}$ , (c) distribution of  $V_s^{30}$ , interpolated from the Taiwan region from the Engineering Geological Database for TSMIP (solid circles with colors denoting  $V_s^{30}$ ), and (d) impact of the site amplification. (d) The difference between Figure (a) and (b). The unit of the PSHA is PGA (in g) for 10% probability in 50 years (i.e. recurrence interval of 475 years). The locations of the Taipei Basin, Ilan Plain, and Chianan Plain are denoted.

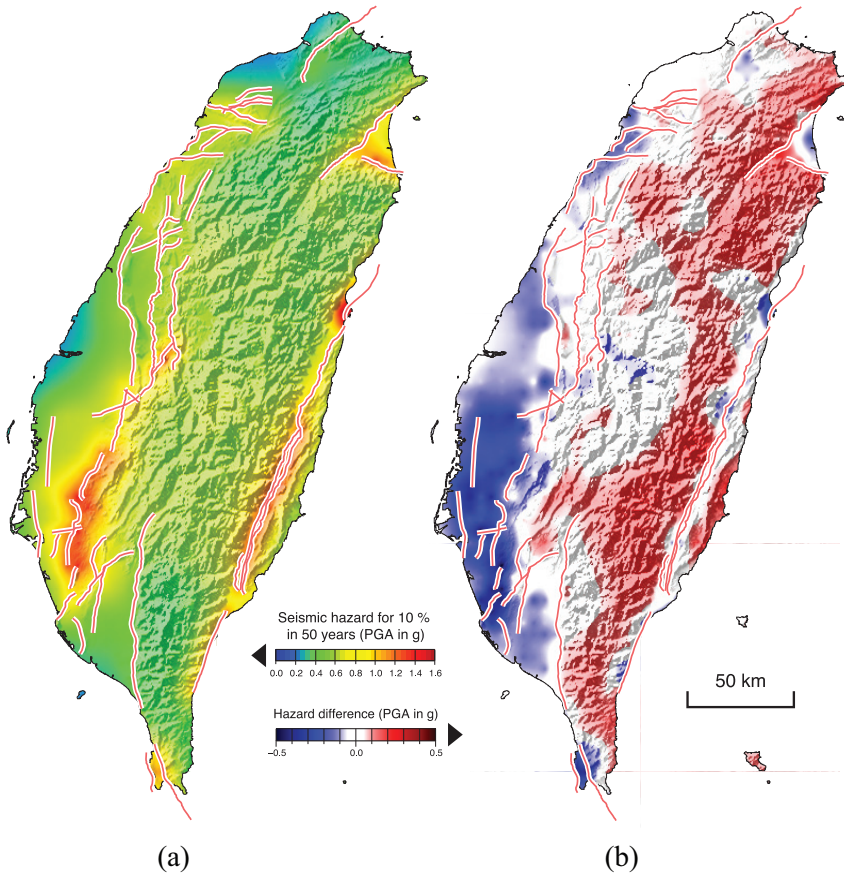


**Figure 8.** (a) The seismic hazard maps considering the ground motion prediction equations proposed by Lin et al. (2011) and (b) the impact of this innovation. (b) The difference between Figures 8a and 7b. The unit of the PSHA is PGA (in g) for 10% probability in 50 years (i.e. recurrence interval of 475 years).

## Discussion

We, as the team of the TEM, have proposed a new PSHA for Taiwan, the TEM PSHA2020. Departing from the previous assessment (TEM PSHA2015), our assessment included several innovations: (1) an updated seismogenic structure database, (2) rupture probability on multiple structures, (3) a time-dependent rupture model for some seismogenic structures, (4) a revised area source model through an updated earthquake catalog, (5) a smoothing model to illustrate background seismicity, and (6) a new set of GMPEs to simulate strong ground motion behaviors. We accessed an updated seismogenic structure database, incorporating six newly identified structure sources (ID 39–44 in Figure 1a) and three-dimensional geometries for some structures (Table 1). And we obtained higher hazard levels in the vicinity of these newly identified structures, whereas some faults with longer rupture return periods (Figure 2) had a lower hazard along them. Considering multiple-structure ruptures did not result in a significant difference in hazard levels for a short return period (e.g. 475 years, corresponding to 10% probability in 50 years), but this factor became crucial when the PSHA return period is assumed to be longer, especially

near the Chaochou fault (ID 29) and the Tainan frontal structure (ID 41), shown in Figure 3. To introduce fault memory of previous events, we adopted the BPT model to evaluate time-dependent earthquake probability. It suggests a higher hazard near the seismogenic structures with longer time elapsed since the last rupture and/or shorter recurrence intervals, such as the Muchiliao-Liuchia (ID 22) and Milun (ID 32) faults. In contrast, earthquake probabilities for the structures with recent events, for example, the Chelungpu fault (ID 17) after the 1999 earthquake, become lower, resulting in a lower hazard level in their vicinities (Figure 4). The treatment of the background seismicity activity is based on the updated earthquake catalog (Figure 5) for implementing both area source (Figure 6a) and smoothing (Figure 6b) models. To be easily applied by various end users, the TEM PSHA2020 included two versions: one based on engineering bedrock (Figure 7a) and the other on built-in site amplification, considering an  $V_s^{30}$  map (Figure 7b).

Our analyses including site effect have a significant impact on hazard levels and warned of high hazard potential in the Taipei Basin, Ilan Basin, and Chianan Plain (Figure 7). Furthermore, the Central Geological Survey has identified most of these regions having high soil liquefaction potential (<https://www.liquid.net.tw/CGS/Web/Map.aspx>), which might be triggered by strong ground shaking during an earthquake, resulting in a secondary hazard. Thus, a reliable  $V_s^{30}$  map is crucial for hazard assessment. The site condition utilized in this study was based on the on-site surveys on the TSMIP station sites (Kuo et al., 2012, and references therein), that is, the sites of interest that are far from a TSMIP site obtain a less precise  $V_s^{30}$ . In addition, the  $V_s^{30}$  map we obtained (Figure 7c) is simply based on interpolation, that is, geological and topographic information was not incorporated. Anyone wanting to obtain a more reliable  $V_s^{30}$  map could follow the model proposed by Kwok et al. (2018) that is based on geological classification and topographic gradient. Alternatively, it is desired to implement an  $V_s^{30}$  obtained by an on-site survey, such as a microtremor survey and/or standard penetration test.

## Conclusion

Since the implemented innovations are based on an up-to-date database and our work could provide a more reliable hazard assessment for Taiwan that could be widely applied for various aspects. Our hazard assessment includes site amplification (Figure 9b and d), which could be widely applied by non-experts without science or engineering backgrounds, such some as in government agencies (e.g. the National Science and Technology Center for Disaster Reduction). In addition, we are aware that some applications do not require this factor (e.g. building code legislation, engineering purposes). Thus, we also provide the hazard maps without site effects (Figure 9a and c); end users could incorporate site amplifications on their own.

While we have just proposed a new version of PSHA for Taiwan, we already expect to make some updates in the next generation of the TEM PSHA. For example, the current PSHA followed the TEM PSHA2015 for the subduction source model. An update could include outcomes of the Reevaluation of Probabilistic Seismic Hazard of Nuclear Facilities in Taiwan Using SSHAC Level 3 Methodology. Although we have updated the seismogenic structure database based on state-of-the-art geomorphology and geology studies (Shyu et al., 2020), we will incorporate seismogenic parameters obtained from geodetic research. In respect to the GMPEs, some new sets of GMPEs, for example, Chao et al. (2020) and Phung et al. (2020), will be discussed, and their epistemic uncertainties (Phung et al., 2019) will be evaluated and considered in a logic tree.

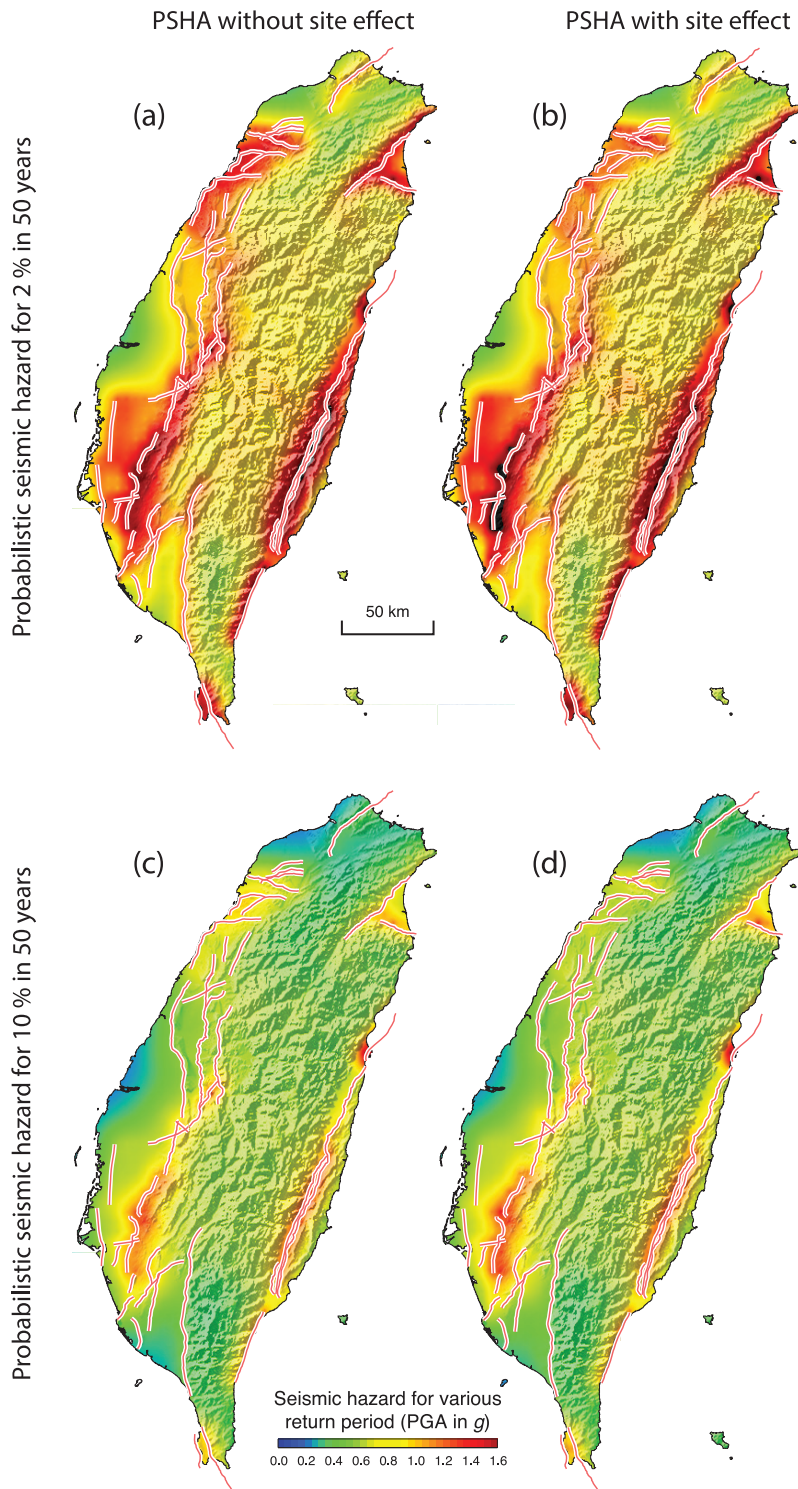


**Figure 9.** The hazard maps of the TEM PSHA2020, considering (a, c) engineering bedrock and (b, d) site amplification for (a, b) 2% and (c, d) 10% probability in 50 years in PGA (in  $g$ ).


## Declaration of conflicting interests

The author(s) declared no potential conflicts of interest with respect to the research, authorship, and/or publication of this article.

## Funding

The author(s) disclosed receipt of the following financial support for the research, authorship, and/or publication of this article: This study was supported by the TEM, and funded by the Ministry of Science and Technology—under the grants MOST 107-2119-M-006-011 and MOST 108-2119-M-006-004—and by the National Research Foundation Singapore and the Singapore Ministry of Education under the Research Centers of Excellence initiative. The seismic hazard calculations were conducted by the open source software OpenQuake, developed by the Global Earthquake Model.

## ORCID iD

Yin-Tung Yen  <https://orcid.org/0000-0003-1338-3592>

## References

- Chan CH, Ma KF, Lee YT and Wang YJ (2019) Rethinking seismic source model of probabilistic hazard assessment in Taiwan after the 2018 Hualien, Taiwan, earthquake sequence. *Seismological Research Letters* 90(1): 88–96.
- Chan CH, Wang Y, Wang YJ and Lee YT (2017) Seismic-hazard assessment over time: Modeling earthquakes in Taiwan. *Bulletin of the Seismological Society of America* 107(5): 2342–2352.
- Chao SH, Chiou B, Hsu CC and Lin PS (2020) A horizontal ground-motion model for crustal and subduction earthquakes in Taiwan. *Earthquake Spectra* 36(2): 463–506.
- Chen C-H, Wang J-P, Wu Y-M, Chan C-H and Chang C-H (2013) A study of earthquake inter-occurrence times distribution models in Taiwan. *Natural Hazards* 69(3): 1335–1350.
- Ellsworth WL, Matthews MV, Nadeau RM, Nishenko SP, Reasenberg PA and Simpson RW (1999) *A Physically Based Earthquake Recurrence Model for Estimation of Long-Term Earthquake Probabilities* (U.S. Geological Survey Open-File Report: 99–522). Reston, VA: U.S. Geological Survey.
- Fujiwara H (2014) Seismic hazard maps for Japan. In: Meyers RA (ed.) *Encyclopedia of Complexity and Systems Science*. Berlin: Springer, pp. 1–28.
- Gardner JK and Knopoff L (1974) Is the sequence of earthquakes in Southern California, with aftershocks removed, Poissonian? *Bulletin of the Seismological Society of America* 64(5): 1363–1367.
- Gerstenberger MC, Marzocchi W, Allen T, Pagani M, Adams J, Danciu L, Field EH, Fujiwara H, Luco N, Ma K-F, Meletti C and Petersen MD (2020) Probabilistic seismic hazard analysis at regional and national scale: State of the art and future challenges. *Reviews of Geophysics, AGU Centennial Special Issue* 58: e2019RG000653.
- Gutenberg B and Richter CF (1944) Frequency of earthquakes in California. *Bulletin of the Seismological Society of America* 34(4): 185–188.
- Kuo C-H, Wen K-L, Hsieh H-H, Lin C-M, Chang T-M and Kuo K-W (2012) Site classification and VS30 estimation of free-field TSMIP stations using the logging data of EGD. *Engineering Geology* 129–130: 68–75.
- Kwok OLA, Stewart JP, Kwak DY and Sun PL (2018) Taiwan-specific model for Vs30 prediction considering between-proxy correlations. *Earthquake Spectra* 34(4): 1973–1993.
- Lin PS (2009) *Ground-motion attenuation relationship and path-effect study using Taiwan data set*. PhD Dissertation, Institute of Geophysics, National Central University, Taoyuan City, Taiwan (in Chinese).
- Lin PS, Lee CT, Cheng CT and Sung CH (2011) Response spectral attenuation relations for shallow crustal earthquakes in Taiwan. *Engineering Geology* 121(3–4): 150–164.

- Molchan GM (1990) Strategies in strong earthquake prediction. *Physics of the Earth and Planetary Interiors* 61: 84–98.
- Phung VB, Loh CH, Chao SH and Abrahamson NA (2019) Analysis of epistemic uncertainty associated with GMPEs and their weight within the logic tree for PSHA: Application to Taiwan. *Terrestrial, Atmospheric & Oceanic Sciences* 29: 611–633.
- Phung VB, Loh CH, Chao SH and Abrahamson NA (2020) Ground motion prediction equation for Taiwan subduction zone earthquakes. *Earthquake Spectra* 36(S1): 1331–1358.
- Shyu JBH, Chuang YR, Chen YL, Lee YR and Cheng CT (2016) A new on-land seismogenic structure source database from the Taiwan Earthquake Model (TEM) project for seismic hazard analysis of Taiwan. *Terrestrial, Atmospheric & Oceanic Sciences* 27(3): 311–323.
- Shyu JBH, Yin YH, Chen CH, Chuang YR and Liu SC (2020) Updates to the on-land seismogenic structure source database by the Taiwan Earthquake Model (TEM) project for seismic hazard analysis of Taiwan. *Terrestrial, Atmospheric & Oceanic Sciences*. DOI: 10.3319/TAO.2020.06.08.01. Available at: <http://tao.cgu.org.tw/index.php/articles/archive/geophysics/item/1723-2020060801t>
- Wang YJ, Chan CH, Lee YT, Ma KF, Shyu JBH and Rau RJ (2016a) Probabilistic seismic hazard assessments for Taiwan. *Terrestrial, Atmospheric and Oceanic Sciences* 27(3): 325–340.
- Wang YJ, Lee YT, Chan CH and Ma KF (2016b) An investigation of the reliability of the Taiwan Earthquake Model PSHA2015. *Seismological Research Letters* 87: 1287–1298.
- Woo G (1996) Kernel estimation methods for seismic hazard area source modeling. *Bulletin of the Seismological Society of America* 86: 353–362.
- Wu YM, Chang CH, Zhao L, Teng TL and Nakamura M (2008). A comprehensive relocation of earthquakes in Taiwan from 1991 to 2005. *Bulletin of the Seismological Society of America* 98(3): 1471–1481.